The Effect of Increased Methane Flow Rate on Electronic Correlation of Amorphous Silicon Carbon (a-SiC: H)

soni Prayogi (prayogi.sp@gmail.com)
Universitas Syiah Kuala https://orcid.org/0000-0002-2996-5047
Ayunis Sholehah
Institut Teknologi Sepuluh Nopember
Yoyok Cahyono
Institut Teknologi Sepuluh Nopember
Darminto D
Institut Teknologi Sepuluh Nopember

Research Article

Keywords: a-SiC: H, ES, Flow rate, Methane, p-type, PECVD.

Posted Date: February 23rd, 2021

DOI: https://doi.org/10.21203/rs.3.rs-238543/v1

The Effect of Increased Methane Flow Rate on Electronic Correlation of Amorphous Silicon Carbon (a-SiC: H)

Soni Prayogi[1,2*], Ayunis Sholehah[1], Yoyok Cahyono[1], Darminto D[1,3]
[1]Advanced Materials Research Group, Department of Physics, Institut Teknologi Sepuluh Nopember, Surabaya 60111, Indonesia.
[2]Department of Physics, Syiah Kuala University, Banda Aceh 23111 Indonesia.
[3]Center of Excellence in Automotive Control and System, Institut Teknologi Sepuluh Nopember, Surabaya 60111, Indonesia
prayogi.sp@gmail.com

Abstract

In this study, we report for the first time that the addition of methane (CH_4) flow rate in the p-type a-SiC: H layer greatly affects the electronic correlation in increasing the conversion efficiency of solar cells. The a-SiC: H p-type layer was grown using *Plasma Enhanced Chemical Vapor Deposition* (PECVD) on *Indium Tin Oxide* (ITO) substrate with various methane flow rates. The a-SiC: H p-type layer was characterized including the complex dielectric properties and the complex refractive index using *Ellipsometric Spectroscopy* (ES), while the surface roughness morphology was used *Atomic Force Microscopy* (AFM). In sample P-2 there is a change in the form of a decrease in the value of the refractive index <n> and the E_0 energy in the lower energy compared to the P-1 sample with a change of 0.3 eV, an increase in the optical gap and a decrease in the value of the real and imaginary dielectric function. While the influence of an increase in the carbon composition of the amorphous network order shows the addition of amorphous tissue disorder. Our results, show that the optical magnitude of the p-type a-SiC: H layer is not only affected by the amount of carbon in the film but also the hydrogen which is thought to contribute.

Keywords: a-SiC: H, ES, Flow rate, Methane, p-type, PECVD.

1. Introduction

The p-type layer of a-SiC: H is applied to the solar cell on top lapiasan, the p-type layer in solar cells based on a-SiC: H p-i-n. As a light-receiving layer, p-type layer should be transparent so that the incoming photons more much, which means the carrier concentration increases [1-3]. In order for the p-type layer to be transparent and able to increase the concentration of the charge carrier, carbon is added when depositing the p-type layer which is made thinner. With the addition of carbon at the time deposed p-type layer, dangling bonds on the wane and become more transparent layers so that the percentage of photons that arrive at the intrinsic layer will increase [4-5]. Therefore, the composition greatly affect the optical gap p-type layer of a-SiC: H.

The optical gap width of the p-type a-SiC: H layer can also be obtained larger in the presence of carbon, besides that the presence of the amount of hydrogen also affects the optical gap increase, so it is often used as a transparent layer that is doped in solar cell applications, sensors, and electrolysis [6-8]. Increasing the width of the optical gap with the presence of carbon in the network layer of the p-type a-SiC: H followed by a worsening of its electrical properties and increased disorder [9-11]. The presence of carbon can increase the width of the state density in the tail region of the energy band, which can decrease the drift mobility thus worsening the electrical properties, whereas the reduction in disorder is thought to be due to the presence of trigonal C=C sp^2 in the sp^3 tetrahedral amorphous network [12-13]. The state density in the tail of the valence and conduction bands is reflected in the slope of the optical absorption curve so that it can be used to determine the electrical properties and amorphous semiconductor disorder. The unfavorable electrical properties are also thought to be related to structural characteristics such as a high number of voids or the formation of certain hydrogen bonds [14]. Therefore, it is necessary to know the structural characteristics and their relationship with the amorphous semiconductor material disorder which affects their electrical properties.

Information about the optical gap of the p-type a-SiC: H layer can be obtained from the optical absorption coefficient α in the visible region, while the optical absorption coefficient α can experimentally be found from the refractive index of the N = n-ik complex as a function of energy [15-16]. Therefore, both the optical magnitude α and n as a function of energy needs to be known in the study of the optical characteristics of the p-type layer of a-SiC: H. This research will study the two optical quantities for the p-type layer a-SiC: H

deposition result by RF-PECVD method. The effect of variations in the flow rate of methane gas on these two optical quantities will be studied with data on the amplitude ratio <ψ> and the phase difference ratio <Δ> between the p and s polarization light waves from the ellipsometric spectroscopy measurements.

2. Experiment Method

In this study, the p-type layer of a-SiC: H grown on *Corning glass 7059* substrate which has been prepared with *Indium Tin Oxide* (ITO). The PECVD technique used consists of two multi-chamber deposition chambers, each of which is specifically used to deposit p-type a-SiC: H layers as shown in Fig 1. In this condition, the filament temperature is only determined by the radiation heater temperature (substrate temperature). Silane gas (SiH_4) with a concentration of 10% in *hydrogen* (H_2) is used as the source gas. Used as a dopant gas *diborane* (B_2H_6) gas concentration of 10% in H_2 for the p-type dopant layer and the addition of *methane* (CH_4) as a p-type layer optimizations that are transparent and capable of increasing the concentration of charge carriers [17]. The growth parameters used are shown in Table 1.

Elipsometric spectroscopy (ES) parameters ψ and Δ (ie, the ratio of the amplitude and the phase difference between the reflected light polarized p and s, respectively) were collected on a 70° angle of incidence, the photon energy range between 0.6 and 6.5 eV using elipsometric spectroscopy (*V-VASE, J. A. Woollam Co*.) with a rotating analyzer and compensator in *Singapore Synchrotron Light Source* (SSLS). In further analysis of the fitting of the measurement data, software is used *Woollam Complete Ease*, with the parameters used in accordance with the surface roughness of the measurement results P-1 and P-2 *Atomic Force Microscopy* (AFM). For each parameter of the dielectric function was evaluated with a combination of *Tauc-Lorentz models* (TL)/*Tauc-Lorntz*+G to determine the thickness, roughness, bandgap, and optical constants p-type layer of a-SiC: H [18].

The following equation is used to analyze the results of elipsometri spectroscopy measurements on the p-type layer of a-SiC: H [19].

1) Complex dielectric functions $\varepsilon\,(\omega) = \varepsilon_1(\omega) + i\varepsilon_2(\omega)$ (ω = the angular frequency of the incident photon).
2) Refractive index $n\,(\omega) = \sqrt{\frac{1}{2}[\sqrt{\varepsilon_1^2(\omega) + \varepsilon_2^2(\omega)} + \varepsilon_1(\omega)]}$

3) Extinction coefficient $\kappa\,(\omega) = \sqrt{\frac{1}{2}[\sqrt{\varepsilon_1^2(\omega) + \varepsilon_2^2(\omega)} - \varepsilon_1(\omega)]}$

4) Loss function $-Im\,[\varepsilon^{-1}(\omega)] = \frac{\varepsilon_2(\omega)}{[\varepsilon_1^2(\omega)+\varepsilon_2^2(\omega)]}$

5) The reflectivity of normal incidence $R\,(\omega) = \frac{[n(\omega)-1]^2+\kappa^2(\omega)}{[n(\omega)+1]^2+\kappa^2(\omega)}$

3. Result and Discussion

Measurement <ψ> and <Δ> of ellipsometric spectroscopy for samples of P-1 and P-2 show in Fig 2 along with the results of data fitting. To support the optical and electronic analysis of each sample, obtained from the sample surface roughness of P-1 and P-2 as in Fig 3. which showed the surface morphology of P-1 and P-2 on 2x2 μm^2 film area. In the P1 and P-2 samples it is seen that they are very uniform across the samples. Where the small grain size was observed in samples of P-1 and the grain size is increased in samples of P-2. This is due to changes in the nucleation process and growth in the sample with the addition of the methane flow rate. The *root-mean-square* (RMS) surface roughness values of the samples obtained from AFM measurements were found to be 8.95 and 6.20 nm according to sample P-1 and sample P-2.

The p-type layer of a-SiC: H were measured at room temperature in the optical energy range 0.6-6.6 eV. From the results of the sample fitting P-1 and P-2 obtained information and parameters of the optical properties of materials, such as refractive index, dielectric constant, the absorption coefficient, thickness and roughness p-type layer of a-SiC: H. Furthermore, from the *complex dielectric function* <ε_1> and <ε_2> obtained *loss-function*, as well as *optical conductivity* <σ_1> and from *refractive index* <n> and *extinction coefficient* <k> obtained *normal incident reflectivity* <R> of each sample [20].

3.1 Complex dielectric function <ε_1> and <ε_2>

The dielectric function <ε> describes the optical and electrical properties of the material over the measurement energy range. Dielectric function consists of two components, namely the real <ε_1> and imaginary <ε_2>. The real component <ε_1> represents the polarization of the material due to the electric dipole which contributes to the atomic and electric polarization, while the imaginary component <ε_2> represents the amount of light absorption in the material [21]. In Fig 4 the real component <ε_1> shows the value of E_0 in sample P-1 of 2.94 eV and sample P-2 of 2.64 eV. Where there is a change in E_0 energy in sample P-2 changes in energy to be smaller than sample P-1 with a large change of 0.3 eV, this proves that at that energy P-

2 sample can absorb more energy than sample P-1 and ultimately to improve the performance of the p-type layer on the solar cell based p-i-n a-SiC: H. The same is true for the imaginary component <ε_2> the values of E_1 and E_2 which are characteristic of the excitability of each sample, showing that in sample P-2 the values of E_1 and E_2 change at a smaller energy than that of sample P-1.

3.2 Refractive index <n> and Extinction coefficient <k>

The values of the complex refractive index <*n*> and <*k*> obtained through ellipsometric spectroscopic measurements represent the <*n*> value which represents the refractive index of the material and the <*k*> value which represents the extinction coefficient of material absorption and energy lost due to the scattering process [22]. Figure 5 shows the optical properties of the sample layer P-1 and P-2 for measurements at the same temperature on the substrate ITO. In the P-2 sample, the p-type a-SiC: H layer quality was quite good in terms of the lowest n value compared to the P-1 sample. At energy <3.0 eV in <*n*> sample P-2, there is a very sharp decrease compared to sample P-1, this shows that the maximum absorption rate obtained is greater for sample P-2 than for sample P-1 even though for each sample it is measured at the same substrate temperature. During deposition, the substrate temperature greatly affects the diffusion process of the deposited atoms on the substrate. In this case because the temperature of the substrate will cause the atoms of the surface of the substrate to vibrate and as a result, the distance between the planes stretches, making the insertion process easier.

In the extinction coefficient <*k*> in sample P-2, it is found that> 3.0 eV is a smaller value than in sample P-1, this indicates that the results of sample P-2 are denser than sample P-1. This shows the extinction coefficient tends to decrease with increasing flow rate of methane gas. Extinction coefficient curves obtained are in limited energy so that it will have an energy price that is owned by a second layer of p-type a-SiC: H. However, at energies> 1.2 eV, a more transparent p-type a-SiC: H layer is produced, this is evidenced by the value of <*k*> which is towards the negative, this is likely to occur saturation of the insertion process of atoms and the result is a layer that is not dense.

3.3 Loss-function $< -Im\,[\varepsilon^{-1}(\omega)] >$ and *Normal incident reflectivity <R>*

Loss-function $< -Im\,[\varepsilon^{-1}(\omega)] >$ as a function of energy can be obtained from the imaginary component <ε_2> and *Normal incident reflectivity <R>* obtained from the real component

<ε_1>[23], as shown in Fig 6 for both P-1 and P-2 samples. The figure shows a shift in the curve $< -Im\,[\varepsilon^{-1}(\omega)] >$ to a higher energy at P-2 with increasing methane gas flow rate. The shift is due to the influence of the flow rate of methane gas, whereas here there is a relationship between a shift to a higher energy and an increase in carbon concentration. The optical gap of the a-SiC: H p-type layer can be obtained from the curve *Normal incident reflectivity* <*R*> by using the definition of energy E_g, namely the definition of energy at the moment *Normal incident reflectivity* <*R*> valuable >3.0 eV.

The band structure model of the p-type a-SiC: H layer in the results of this study is illustrated as in Fig 8 for samples P-1 and P-2. Increasing the flow rate of methane increase the amount of carbon in the p-type layer of a-SiC: H. N_H determining the concentration of hydrogen contained in the p-type layer of a-SiC: H obtained from the experimental results of hydrogen effusion. Increasing the flow rate of methane gas also increases the concentration of hydrogen in addition to the amount of carbon in the p-type layer of a-SiC: H. Therefore, the effect of the flow rate of methane gas on the optical quantities stated above is due to the influence of carbon and hydrogen. The optical magnitude of the refractive index <n> and the optical gap Eg will be related to the amount of hydrogen and carbon in the p-type layer as shown in Fig 8. The figure shows that both carbon and hydrogen have an effect on reducing the refractive index <*n*> and increasing the optical gap E_g. Most researchers attribute increasing the optical gap to increasing carbon concentration alone, but hydrogen also has an effect. Likewise with the reduced refractive index <*n*> which most researchers associated with an increase in carbon concentration, even though the deposition process uses methane gas as a carbon source.

4. Conclusion

The effect of variations in the flow rate of methane gas on the optical characteristics of the p-type layer a-SiC: H deposition results from the PECVD technique shows changes in the form of a decrease in the value of the refractive index <*n*> and the E_0 energy in sample P-2 changes in energy to a smaller one than the sample P-1 with a change of 0.3 eV, an increase in the optical gap and a decrease in the value of the dielectric function of the real and imaginary parts. Meanwhile, the effect of increasing carbon composition on the regularity of amorphous tissue shows the addition of amorphous tissue disorder. The magnitude of the optical layer of the p-type a-SiC: H is not only influenced by the amount of carbon in the film but also hydrogen which is estimated to have contributed.

5. Acknowledgment

The author thankfully acknowledges the Ministry of Finance of the Republic of Indonesian, through the Lembaga Pengelolah Dana Pendidikan (LPDP), which has provided financial support through the Scholarship Indonesian. The authors would also appreciate LPPM Institut Teknologi Sepuluh Nopember for the use of experimental facilities at Research Center ITS. We also acknowledge the NUS Singapore Synchrotron Light Source (SSLS) SE measurements. We are thankful to Prof. Andrivo Rusydi *National University of Singapore* who provided a fruitful discussion for this paper.

6. References

1. R. Saleh and N. H. Nickel, "The influence of Fermi energy on structural and electrical properties of laser crystallized P-doped amorphous silicon," *Appl. Surf. Sci.*, vol. 254, no. 11, pp. 3324–3330, Mar. 2008, https://doi.org/10.1016/j.apsusc.2007.11.011.
2. Kundu, K., Ghosh, A., Ray, A. *et al.* Boron-doped silicon carbide (SiC) thin film on silicon (Si): a novel electrode material for supercapacitor application. *J Mater Sci: Mater Electron* 31**,** 17943–17952 (2020). https://doi.org/10.1007/s10854-020-04346-y.
3. Budaguan, B.G., Sherchenkov, A.A., Berdnikov, A.E. *et al.* The Properties of a-SiC:H and a-SiGe:H Films Deposited by 55 kHz PECVD. *MRS Online Proceedings Library* 557**,** 43–48 (1999). https://doi.org/10.1557/PROC-557-43.
4. S. Prayogi, Ayunis, Kresna, Y. Cahyono, Akidah, and Darminto, "Analysis of thin layer optical properties of a-Si:H P-Type doping CH_4 and P-Type without CH_4 is deposited PECVD systems," *J. Phys. Conf. Ser.*, vol. 853, p. 012032, May 2017, https://doi.org/10.1088/1742-6596/853/1/012032.
5. Ouwens, J.D., Schropp, R., Van Der Werf, C. *et al.* Effects of Electrode Spacing and Hydrogen Dilution on *a*-SiC:H and *a*-Si:H Layers. *MRS Online Proceedings Library* 297**,** 61–66 (1993). https://doi.org/10.1557/PROC-297-61.
6. R. Saleh and N. H. Nickel, "Boron Doped Polycrystalline Silicon Produced By Step-by-Step XeCl Excimer Laser Crystallization," *MRS Online Proc. Libr. OPL*, vol. 910, ed 2006, https://doi.org/10.1557/PROC-0910-A23-02.
7. Nebel, C., Street, R. Revealing Mysteries of Hall Experiments on a-Si:H and a-SiC:H. *MRS Online Proceedings Library* 297, 437–442 (1993). https://doi.org/10.1557/PROC-297-437.
8. Hanidu G.A., Banerjee P.K., Kim J.S., Mitra S.S. (1989) Vibrational and Electrical Properties of n and p Doped a-SiC:H Films. In: Rahman M.M., Yang C.YW., Harris G.L. (eds) Amorphous and Crystalline Silicon Carbide II. Springer Proceedings in Physics, vol 43. Springer, Berlin, Heidelberg. https://doi.org/10.1007/978-3-642-75048-9_26.
9. R. Saleh and N. H. Nickel, "Silicon-Hydrogen Bonds in Boron and Phosphorous Doped Polycrystalline Silicon Thin Films," *MRS Online Proc. Libr. OPL*, vol. 808, ed 2004, https://doi.org/10.1557/PROC-808-A4.4.

10. Nakanishi, T., Marukawa, Y., Takahashi, S. *et al.* Deposition Kinetics of a-Si:H and a-SiC:H for Fabrication of a-Si / a-SiC Double-Layered Photoreceptor. *MRS Online Proceedings Library* 118, 55 (1988). https://doi.org/10.1557/PROC-118-55.
11. Sánchez-Garrido, O., Gómez-Aleixandre, C., Olías, J.S. *et al.* Dielectric and Raman spectroscopy of MWCVD diamond thin films. *J Mater Sci: Mater Electron* **7,** 297–303 (1996). https://doi.org/10.1007/BF00188958.
12. Y. Cahyono, U. Maslakah, F. D. Muttaqin, and Darminto, "Reduced energy bandgap of a-Si:H films deposited by PECVD at elevating temperatures," *AIP Conf. Proc.*, vol. 1801, no. 1, p. 020008, Jan. 2017, https://doi.org/10.1063/1.4973086.
13. Das, G., Mandal, S., Mukhopadhyay, S. *et al.* Effect of oxide based graded buffer and bottom n-layer on the performance of the single junction amorphous silicon solar cells. *J Mater Sci: Mater Electron* 28, 16165–16172 (2017). https://doi.org/10.1007/s10854-017-7517-y.
14. R. Gogolin *et al.*, "Analysis of Series Resistance Losses in a-Si:H/c-Si Heterojunction Solar Cells," *IEEE J. Photovolt.*, vol. 4, no. 5, pp. 1169–1176, Sep. 2014, https://doi.org/10.1109/JPHOTOV.2014.2328575.
15. J. Tauc, R. Grigorovici, and A. Vancu, "Optical Properties and Electronic Structure of Amorphous Germanium," *Phys. Status Solidi B*, vol. 15, no. 2, pp. 627–637, 1966, https://doi.org/10.1002/pssb.19660150224.
16. Szklarska-Smialowska Z., Krishnakumar R. (1991) Ellipsometry in Studies of Metallic Corrosion and Oxidation. In: Ferreira M.G.S., Melendres C.A. (eds) Electrochemical and Optical Techniques for the Study and Monitoring of Metallic Corrosion. NATO ASI Series (Series E: Applied Sciences), vol 203. Springer, Dordrecht. https://doi.org/10.1007/978-94-011-3636-5_9.
17. S. Prayogi, M. A. Baqiya, Y. Cahyono, and Darminto, "Optical Transmission of p-Type a-Si:H Thin Film Deposited by PECVD on ITO-Coated Glass," *Materials Science Forum*, 2019. https://www.scientific.net/MSF.966.72.
18. M. H. Brodsky, R. S. Title, K. Weiser, and G. D. Pettit, "Structural, Optical, and Electrical Properties of Amorphous Silicon Films," *Phys. Rev. B*, vol. 1, no. 6, pp. 2632–2641, Mar. 1970, https://doi.org/10.1103/PhysRevB.1.2632.
19. A. Chaudhuri *et al.*, "Quasilocal plasmons in the insulator-metal transition in the Mott-type perovskites," *Phys. Rev. B*, vol. 98, no. 16, p. 165303, Oct. 2018, https://doi.org/10.1103/PhysRevB.98.165303.
20. P. K. Das *et al.*, "Electronic correlation determining correlated plasmons in Sb-doped," *Phys. Rev. B*, vol. 100, no. 11, p. 115109, Sep. 2019, https://doi.org/10.1103/PhysRevB.100.115109.
21. G. E. Jellison and F. A. Modine, "Parameterization of the optical functions of amorphous materials in the interband region," *Appl. Phys. Lett.*, vol. 69, no. 3, pp. 371–373, Jul. 1996, https://doi.org/10.1063/1.118064.
22. J. D. Joannopoulos and M. L. Cohen, "Electronic Properties of Complex Crystalline and Amorphous Phases of Ge and Si. I. Density of States and Band Structures," *Phys. Rev. B*, vol. 7, no. 6, pp. 2644–2657, Mar. 1973, https://doi.org/10.1103/PhysRevB.7.2644.
23. X. Yin *et al.*, "Quantum Correlated Plasmons and Their Tunability in Undoped and Doped Mott-Insulator Cuprates," *ACS Photonics*, vol. 6, no. 12, pp. 3281–3289, Dec. 2019, https://doi.org/10.1021/acsphotonics.9b01294.

Figures caption

Figure 1 :Schematic of p-type a-SiC: H deposition sample preparation

Figure 2 :Experimental data (*solid curve*) and fittings (*point curve*) from <Ψ> and <**Δ**> to (a) P-1, and (b) P-2. Obtained by measurement by angle 70^{o}.

Figure 3 :Surface roughness (a) P-1 and (b) P-2. Measurement results with AFM.

Figure 4 :(a) Real part <ε1>, and (b) imaginary part <ε2>. From the dielectric function for P-1 and P-2 sample a-SiC: H.

Figure 5 :Complex refractive index (a) <*n*> and (b) <*k*> for samples P-1 and P-2 sample a-SiC: H

Figure 6 :(a) Loss-function and (b) Reflectivity for samples P-1 and P-2 sample a-SiC: H.

Figure 7 :Possible band-structure scheme in P-1 and P-2. E_F denotes fermi level. Thickness of arrows qualitatively indicates strength of the transitions

Figure 1

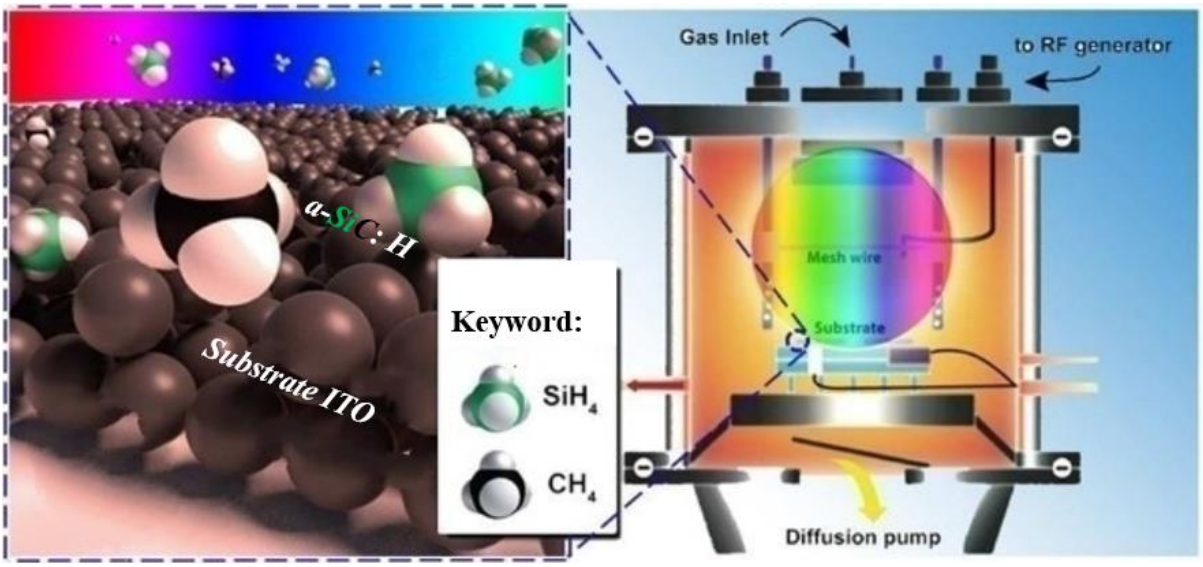
a-SiC: H
Substrate ITO
Keyword:
SiH4
CH4
Gas Inlet
to RF generator
Mesh wire
Substrate
Diffusion pump

Figure 2

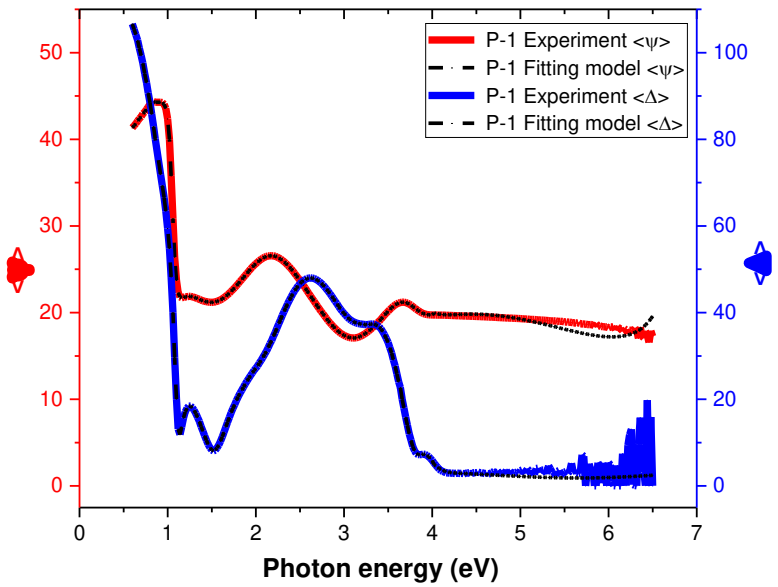
P-1 Experiment <ψ>
P-1 Fitting model <ψ>
P-1 Experiment <Δ>
P-1 Fitting model <Δ>
Photon energy (eV)

(a)

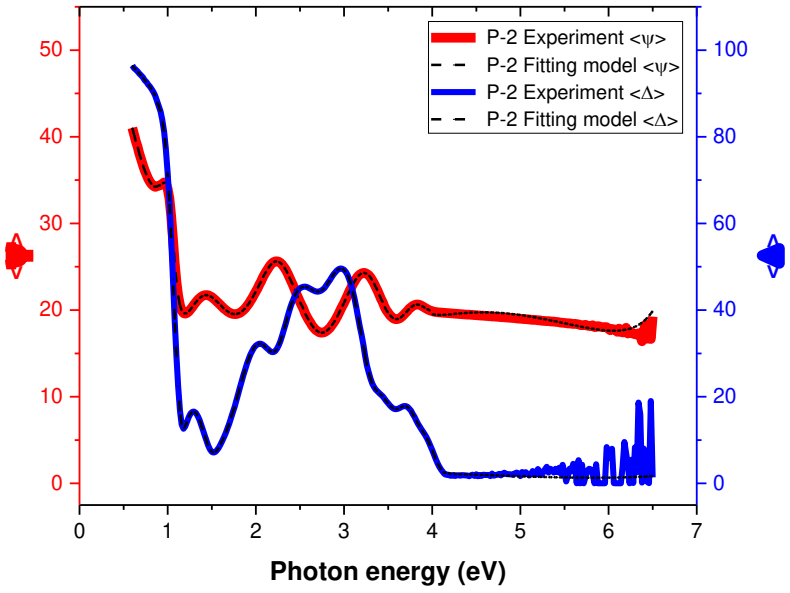
P-2 Experiment <ψ>
P-2 Fitting model <ψ>
P-2 Experiment <Δ>
P-2 Fitting model <Δ>
Photon energy (eV)

(b)

Figure 3

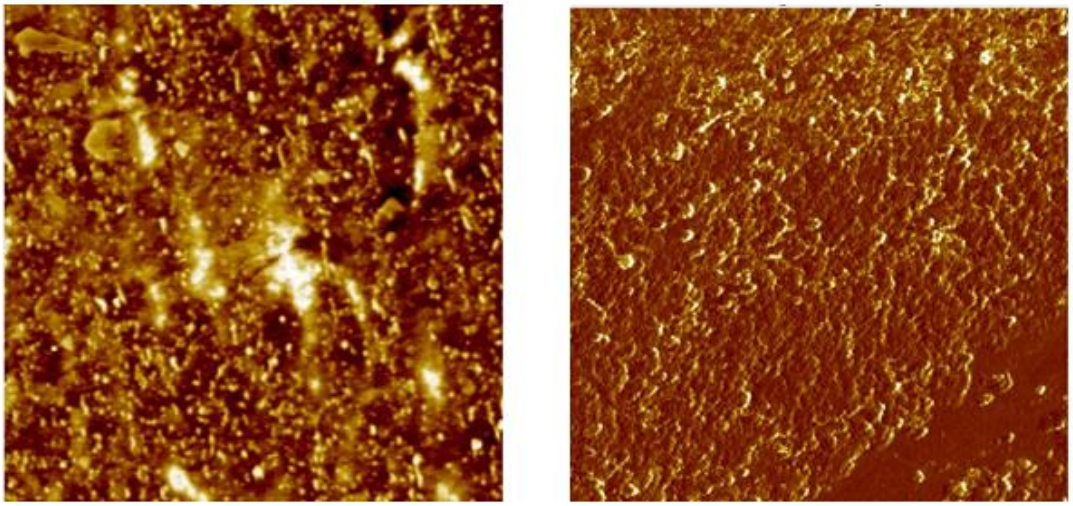

(a) (b)

Figure 4

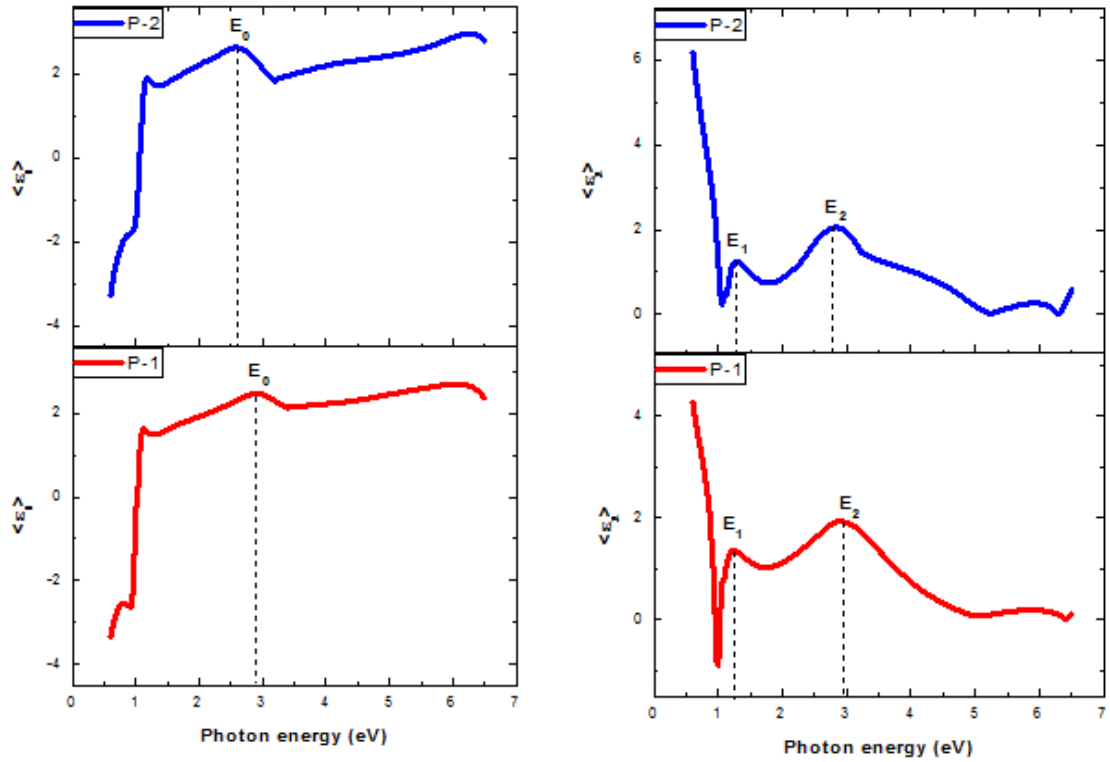
P-2
E0
P-1
E0
<ε1>
Photon energy (eV)
P-2
E1
E2
P-1
E1
E2
<ε2>
Photon energy (eV)

(a) (b)

Figure 5

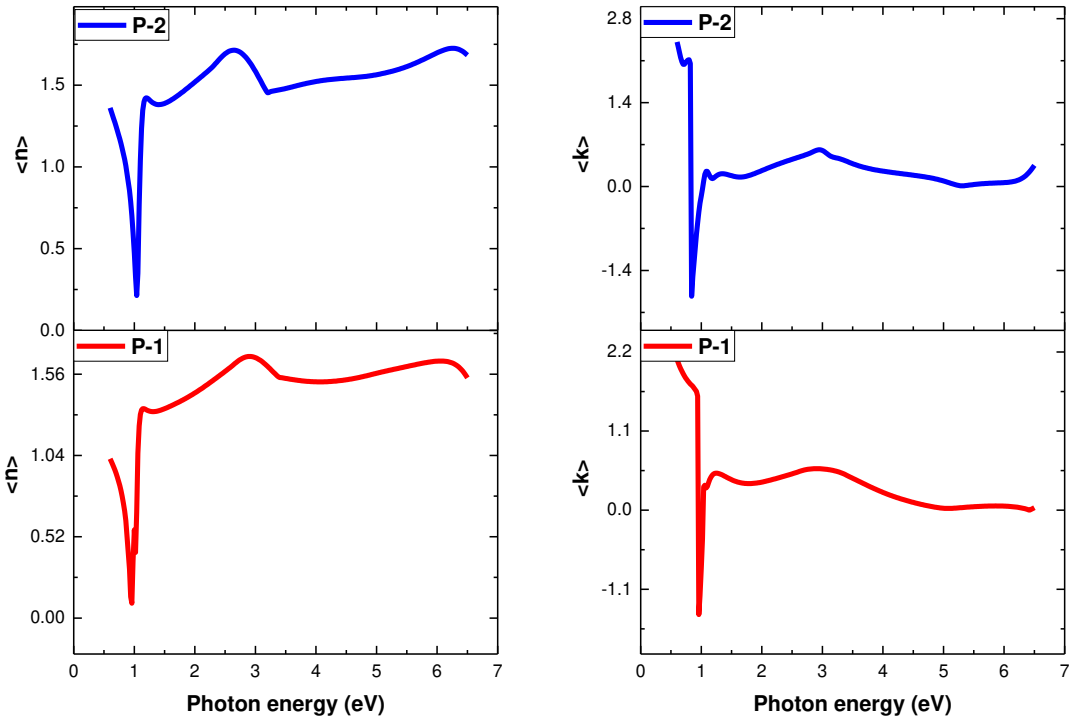
P-2
P-1
<n>
<k>
Photon energy (eV)
0.0
0.5
1.0
1.5
0.00
0.52
1.04
1.56
-1.4
0.0
1.4
2.8
-1.1
0.0
1.1
2.2
0
1
2
3
4
5
6
7

(a) (b)

Figure 6

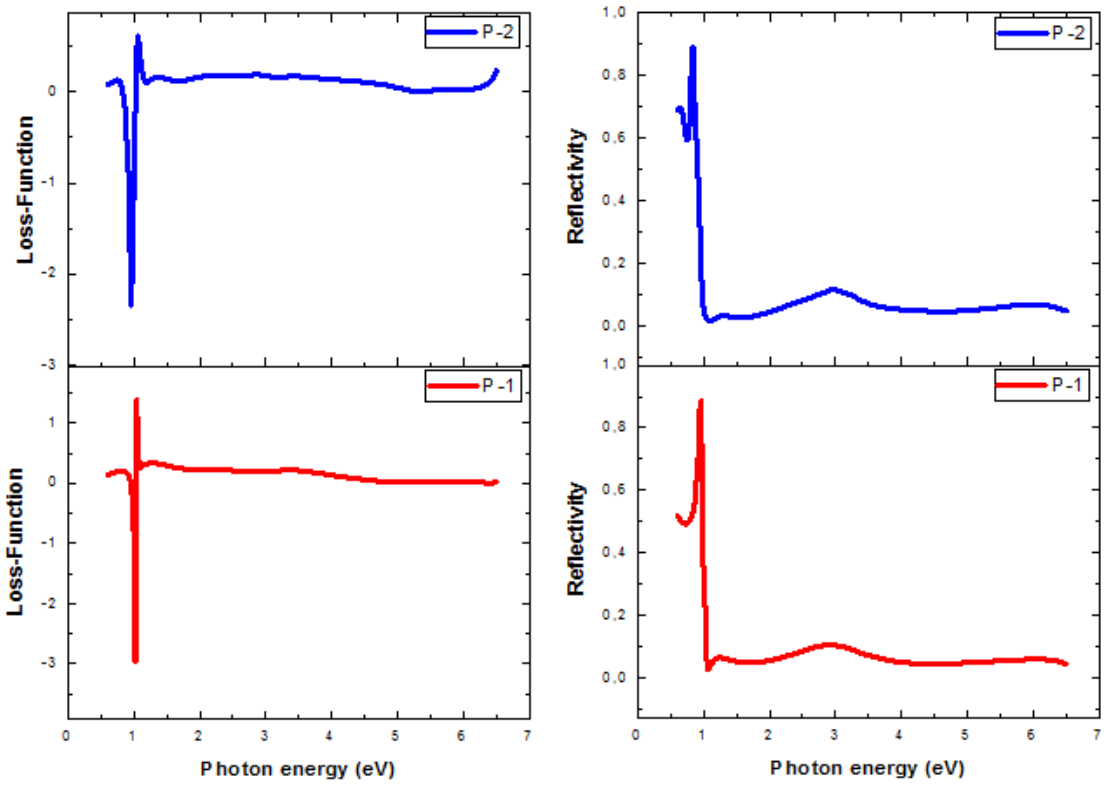

(a) (b)

Figure 7

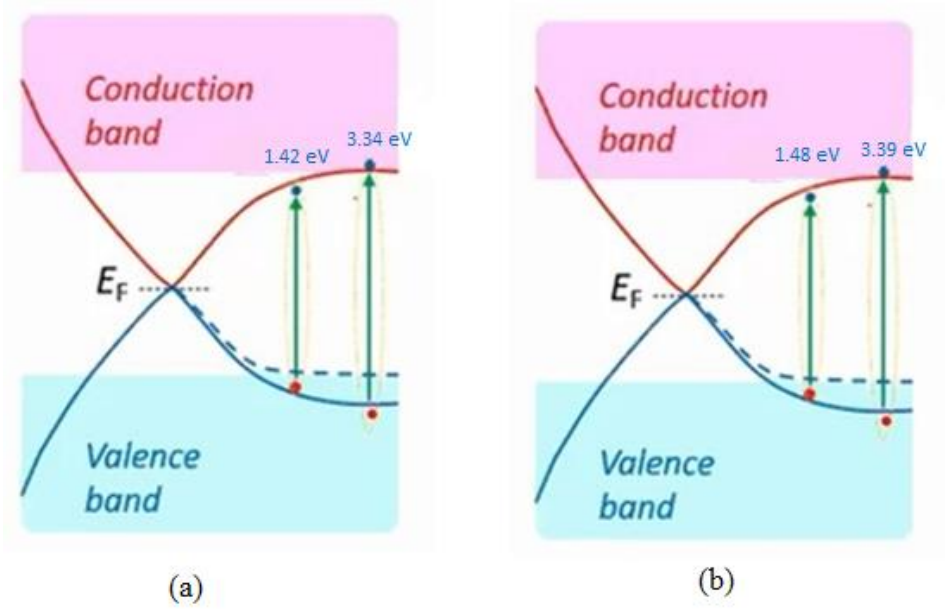
Conduction band
1.42 eV
3.34 eV
E_F
Valence band
(a)
Conduction band
1.48 eV
3.39 eV
E_F
Valence band
(b)

Table 1. Parameters for the deposition of the p-type layer of a-SiC: H

Deposition parameters	**P-type layer of amorphous silicon carbon (a-SiC: H)**	
	P-1	**P-2**
Flow rate S_iH_4	20 sccm	20 sccm
Flow rate B_2H_6	2 sccm	2 sccm
Flow rate H_2	20 sccm	20 sccm
Flow rate CH_4	10 sccm	20 sccm
Power RF	5 Watt	5 Watt
Temperature	210^oC	210^oC
Pressure	4800 mTorr	4800 mTorr
Time	10 Minute	10 Minute

Author declaration

1. Conflict of Interest

Potential conflict of interest exists:

We wish to draw the attention of the Editor to the following facts, which may be considered as potential conflicts of interest, and to significant financial contributions to this work:

The nature of potential conflict of interest is described below:

☒No conflict of interest exists.

We wish to confirm that there are no known conflicts of interest associated with this publication and there has been no significant financial support for this work that could have influenced its outcome.

2. Funding

☒Funding was received for this work.

All of the sources of funding for the work described in this publication are acknowledged below:

[LPDP]

☐No funding was received for this work.

3. Intellectual Property

☒We confirm that we have given due consideration to the protection of intellectual property associated with this work and that there are no impediments to publication, including the timing of publication, with respect to intellectual property. In so doing we confirm that we have followed the regulations of our institutions concerning intellectual property.

4. Research Ethics

☒We further confirm that any aspect of the work covered in this manuscript that has involved human patients has been conducted with the ethical approval of all relevant bodies and that such approvals are acknowledged within the manuscript.

☐IRB approval was obtained (required for studies and series of 3 or more cases)

☐Written consent to publish potentially identifying information, such as details or the case and photographs, was obtained from the patient(s) or their legal guardian(s).

5. Authorship

The Journal of Materials Science: Materials in Electronics (JMSE) recommends that authorship be based on the following four criteria:

1. Substantial contributions to the conception or design of the work; or the acquisition, analysis, or interpretation of data for the work; AND

2. Drafting the work or revising it critically for important intellectual content; AND

3. Final approval of the version to be published; AND

4. Agreement to be accountable for all aspects of the work in ensuring that questions related to the accuracy or integrity of any part of the work are appropriately investigated and resolved.

☒All listed authors meet the JMSE criteria. We attest that all authors contributed significantly to the creation of this manuscript, each having fulfilled criteria as established by the JMSE.

☐One or more listed authors do(es) not meet the JMSE criteria.

We believe these individuals should be listed as authors because:

☐We confirm that the manuscript has been read and approved by all named authors.

☐We confirm that the order of authors listed in the manuscript has been approved by all named authors.

6. Contact with the Editorial Office

The Corresponding Author declared on the title page of the manuscript is:

☒This author submitted this manuscript using his/her account in editorial submission system.

☐We understand that this Corresponding Author is the sole contact for the Editorial process (including the editorial submission system and direct communications with the office). He/she is responsible for communicating with the other authors about progress, submissions of revisions and final approval of proofs.

☐We confirm that the email address shown below is accessible by the Corresponding Author, is the address to which Corresponding Author's editorial submission system account is linked, and has been configured to accept email from the editorial office of International Journal of Women's Dermatology:

[Insert email address you wish to use for communication with the journal here]

☐Someone other than the Corresponding Author declared above submitted this manuscript from his/her account in editorial submission system:

[Insert name below]

☐We understand that this author is the sole contact for the Editorial process (including editorial submission system and direct communications with the office). He/she is responsible for communicating with the other authors, including the Corresponding Author, about progress, submissions of revisions and final approval of proofs.

We the undersigned agree with all of the above.

Author's name (Fist, Last)	Signature	Date
1. *Soni Prayogi*		13/02/2021
2. *Darminto D*		13/02/2021

Figures

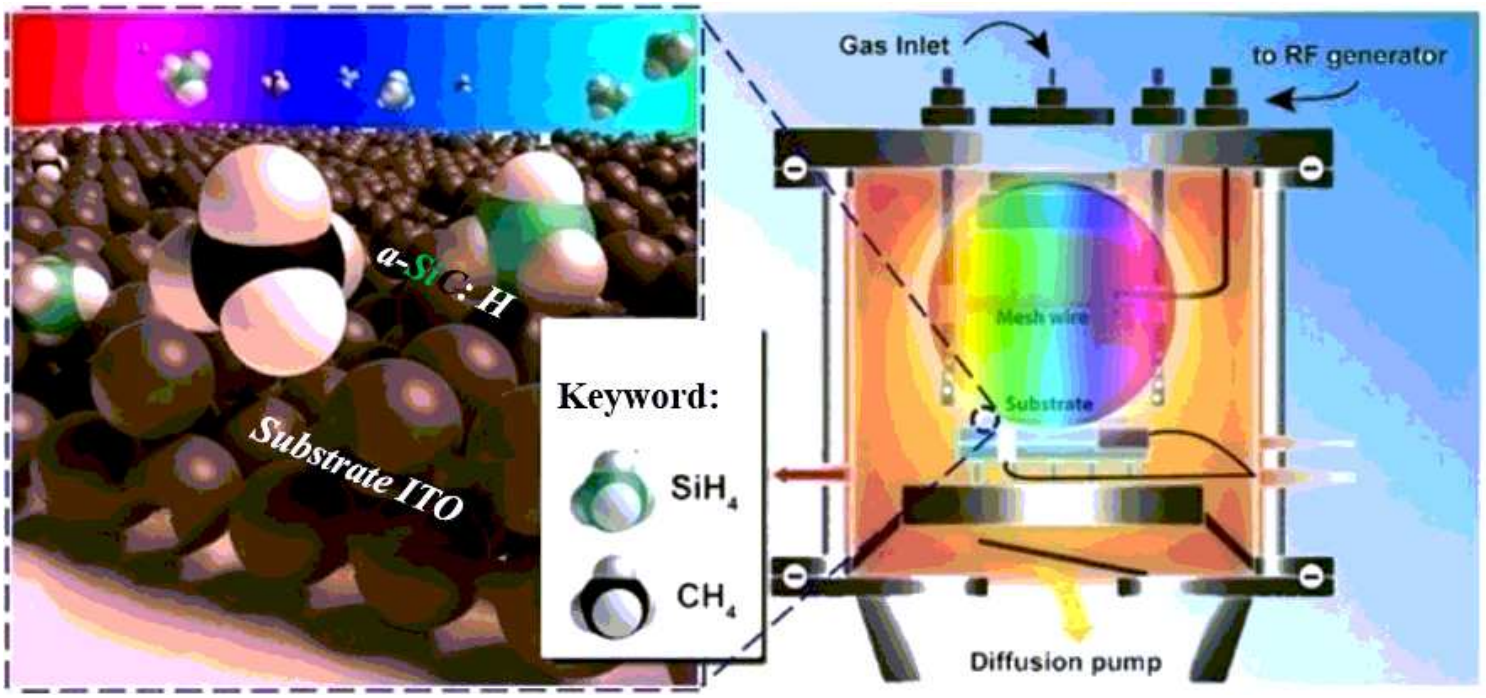

Figure 1

Schematic of p-type a-SiC: H deposition sample preparation

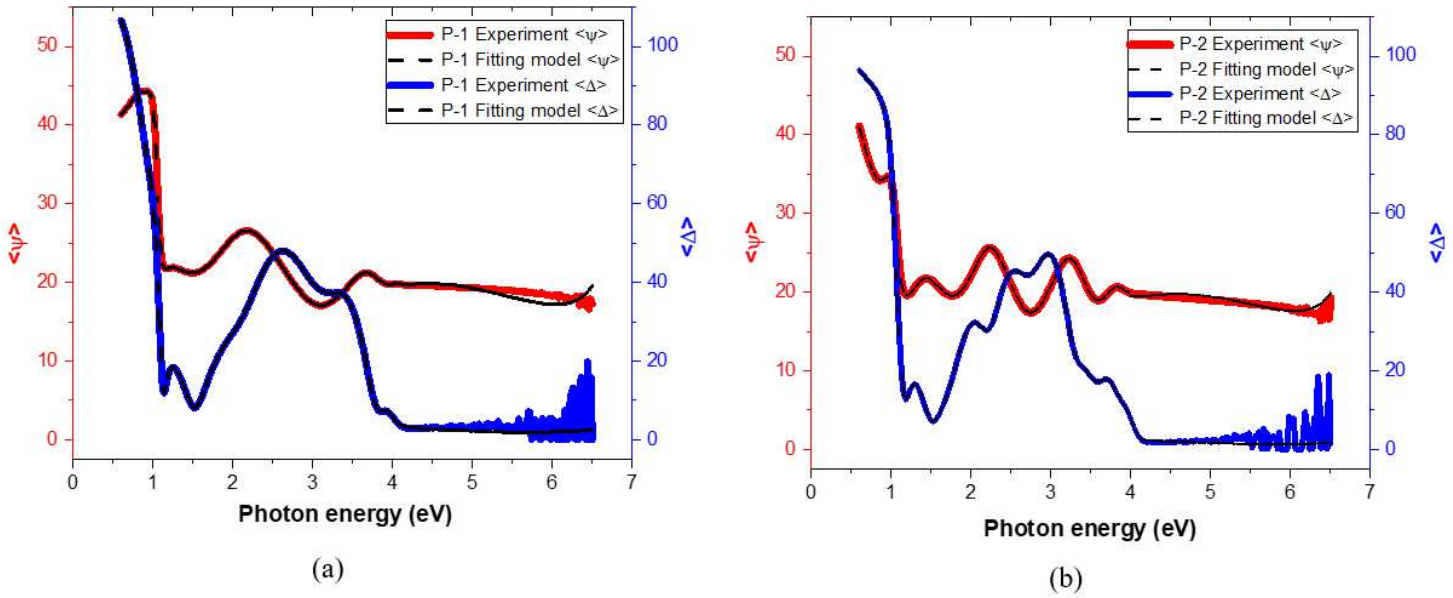

Figure 2

Experimental data (solid curve) and fittings (point curve) from <Ψ> and <□> to (a) P-1, and (b) P-2. Obtained by measurement by angle 70o.

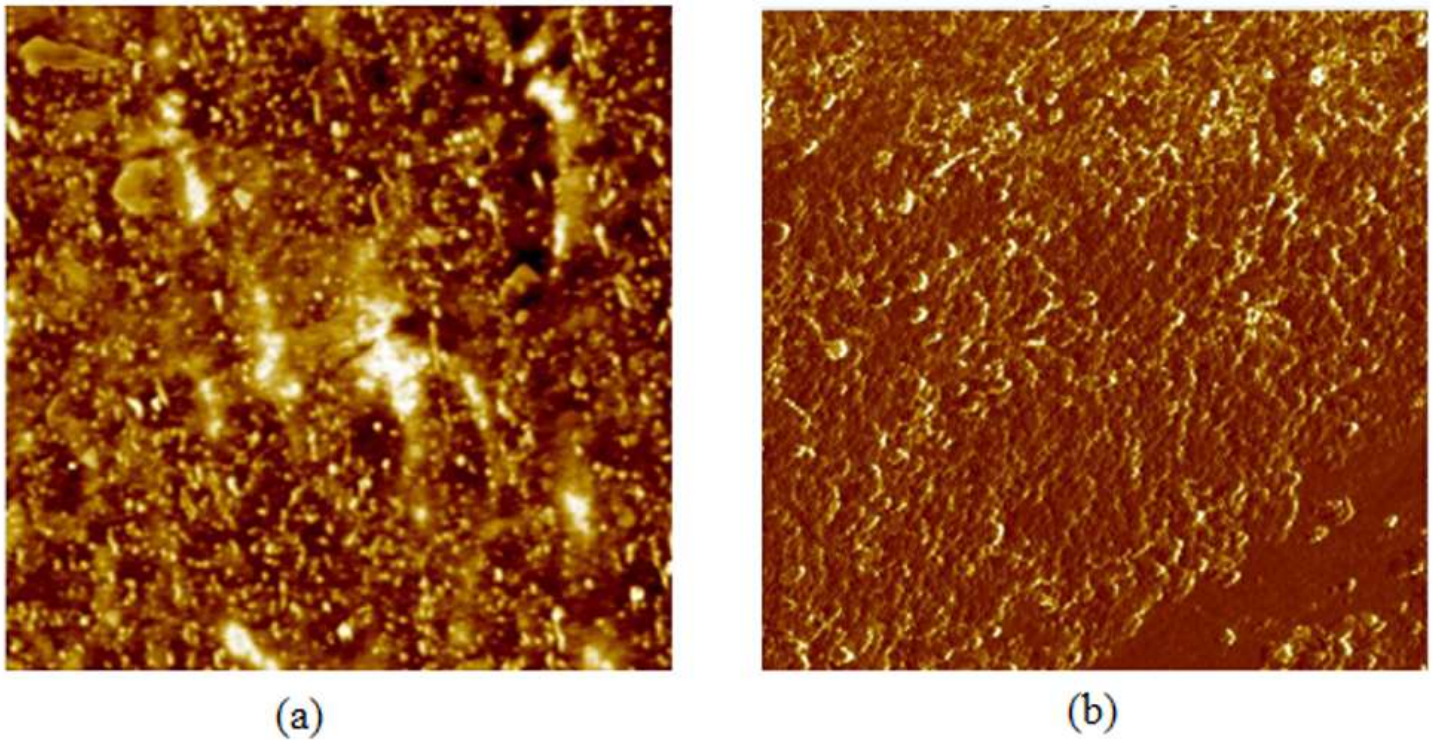

Figure 3

Surface roughness (a) P-1 and (b) P-2. Measurement results with AFM.

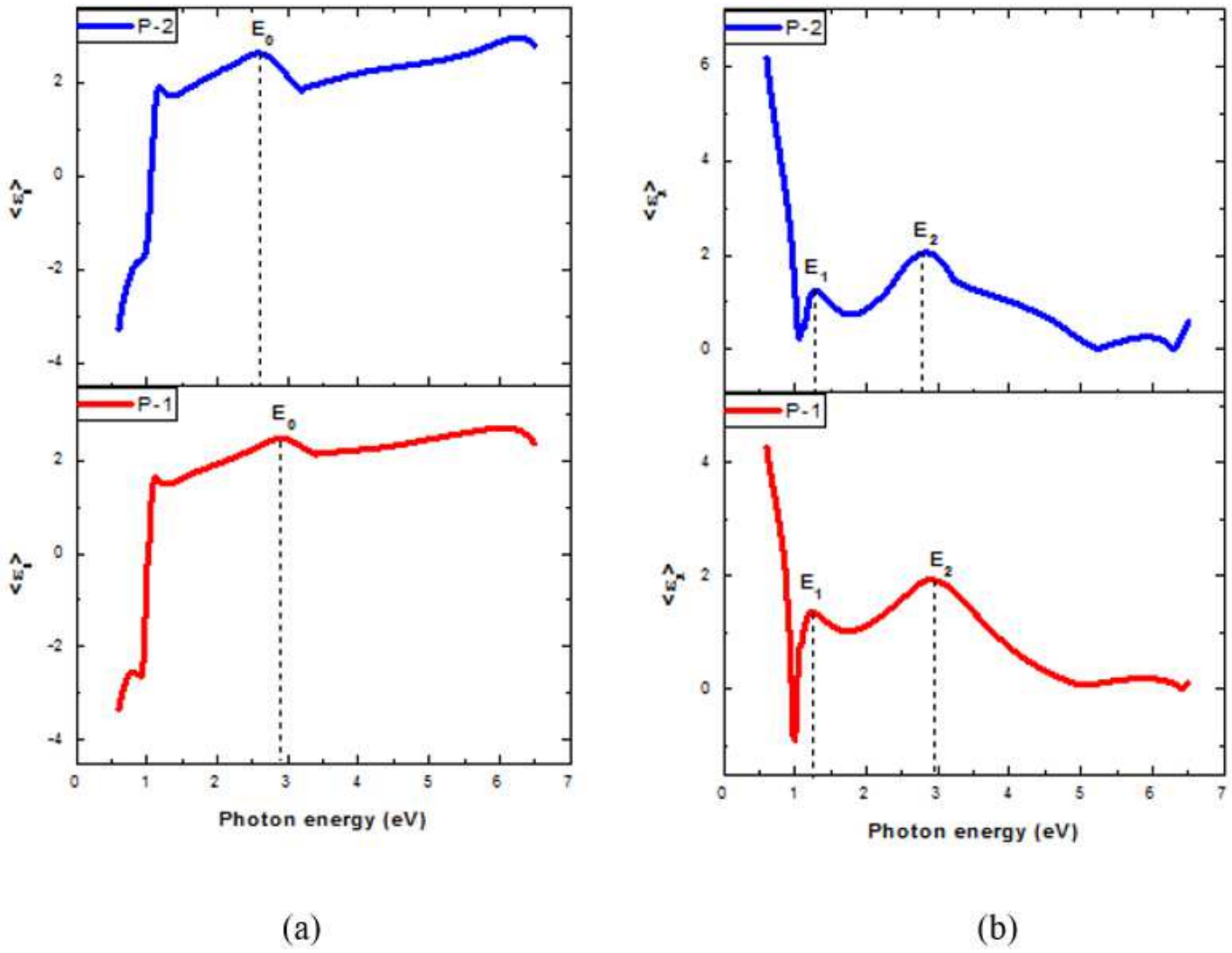

Figure 4

(a) Real part <ε1>, and (b) imaginary part <ε2>. From the dielectric function for P-1 and P-2 sample a-SiC: H.

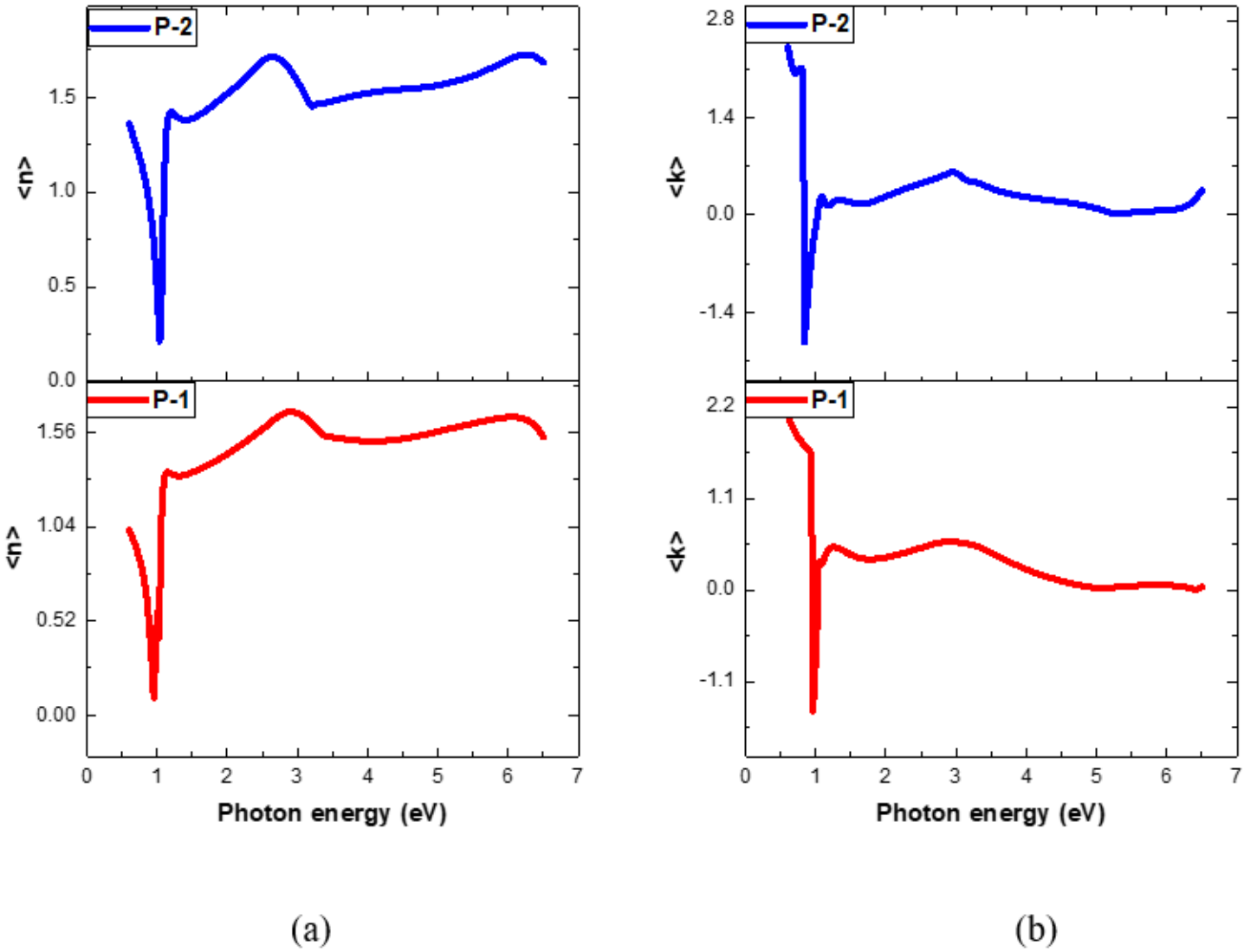

Figure 5

Complex refractive index (a) <n> and (b) <k> for samples P-1 and P-2 sample a-SiC: H

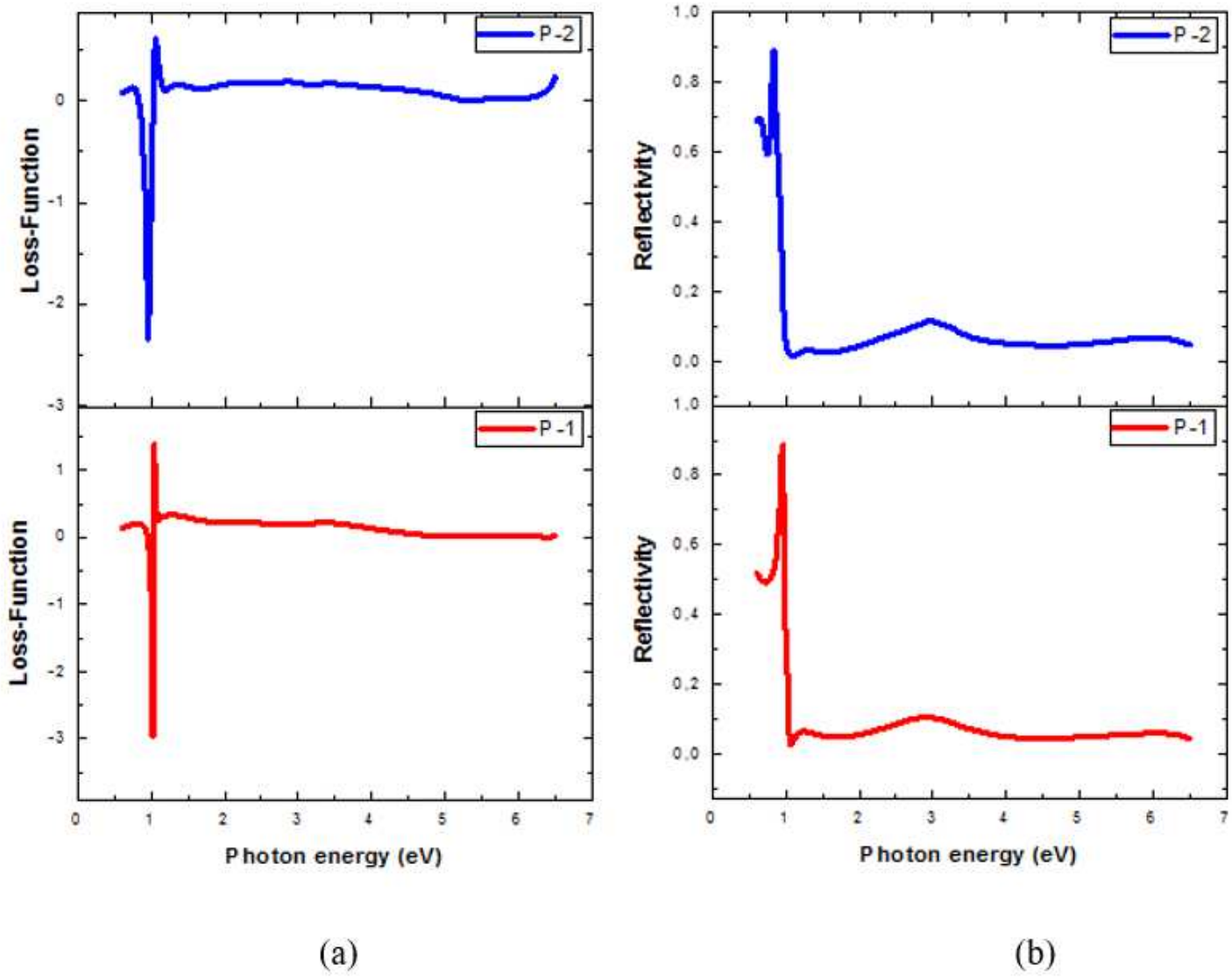

Figure 6

(a) Loss-function and (b) Reflectivity for samples P-1 and P-2 sample a-SiC: H.

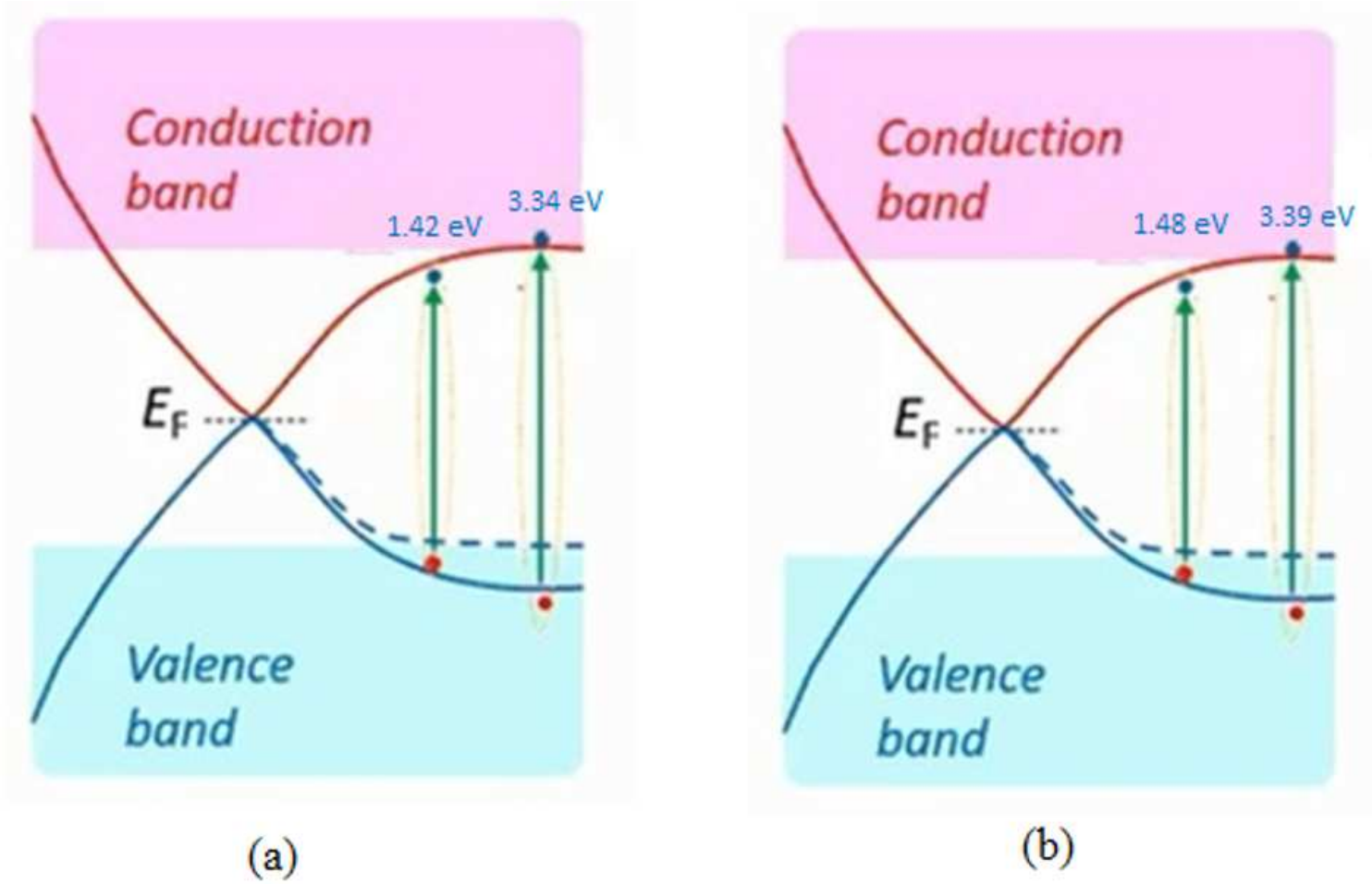

Figure 7

Possible band-structure scheme in P-1 and P-2. EF denotes fermi level. Thickness of arrows qualitatively indicates strength of the transitions